

# Direct Calculation of the Turbulent Dissipation Efficiency in Anelastic Convection

Kaloyan Penev, Joseph Barranco, Dimitar Sasselov, Kaloyan Penev<sup>a</sup>,  
Joseph Barranco<sup>b</sup>, Dimitar Sasselov<sup>c</sup>

<sup>a</sup>60 Garden St., M.S. 10, Cambridge, MA 02138

<sup>b</sup>1600 Holloway Avenue, San Francisco, CA 94132-4163

<sup>c</sup>60 Garden St., M.S. 16, Cambridge, MA 02138

---

## Abstract

The current understanding of the turbulent dissipation in stellar convective zones is based on the assumption that the turbulence follows Kolmogorov scaling. This assumption is valid for some cases in which the time frequency of the external shear is high (e.g. solar p-modes). However, for many cases of astrophysical interest (e.g. binary orbits, stellar pulsations etc.) the timescales of interest lie outside the regime of applicability of Kolmogorov scaling. We present direct calculations of the dissipation efficiency of the turbulent convective flow in this regime using simulations of anelastic convection with external forcing. We show that the effects of the turbulent flow are well represented by an effective viscosity coefficient and we provide the values of the effective viscosity as a function of the perturbation frequency and compare our results to a perturbative method for finding the effective viscosity (based on by Goodman & Oh (1997)) that can be applied to actual simulations of the surface convective zones of stars.

*Key words:* Hydrodynamics, Anelastic approximation, Stratified flows, Shear flows, Spectral methods, Convection, Turbulence, Turbulent dissipation, Effective Viscosity

---

## 1. Introduction

For stars with surface convection, turbulent dissipation in the convective zone is believed to be the dominant mechanism responsible for the conversion of mechanical energy of tides, stellar oscillations and stellar pulsations to heat. Thus, this is the mechanism believed to determine the rates of

tidal synchronization and circularization (Zahn, 1966, 1989), the amplitudes of stellar  $p$  modes (Goldreich & Keeley, 1977; Goldreich & Kumar, 1988; Goldreich et al., 1994), and the instability of stars to pulsations (Gonczi, 1982).

The simplest approach to estimating the dissipation efficiency of the turbulent convection is to assume that the turbulence is homogeneous and isotropic and its interaction with external shear is only local. In that case we can define an effective viscosity coefficient which will capture the effects due to the turbulent flow. The question then is how to find the value of this coefficient.

Currently two prescriptions based on the assumption of Kolmogorov cascade exist for estimating this coefficient as a function of the time period of the external shear ( $T$ ).

Zahn (1966, 1989) proposes that, the effective viscosity should scale linearly with the fraction of a turn eddies manage to complete in half a perturbation period:

$$\nu = \nu_{max} \min \left[ \left( \frac{T}{2\tau} \right), 1 \right]. \quad (1)$$

On the other hand, Goldreich & Nicholson (1977) and Goldreich & Keeley (1977), argue that eddies with turnover times bigger than  $T/2\pi$  will not contribute to the dissipation. Then Kolmogorov scaling predicts:

$$\nu = \nu_{max} \min \left[ \left( \frac{T}{2\pi\tau} \right)^2, 1 \right] \quad (2)$$

Zahn's more efficient dissipation seems to be in better agreement with observations of tidal circularization times for binaries containing a giant star (Verbunt & Phinney, 1995), the location of the red edge of the Cepheid instability strip (Gonczi, 1982), and even this more efficient prescription might be insufficient to explain the main sequence circularization of binary stars in clusters (Meibom & Mathieu, 2005).

However, Goldreich & Keeley (1977), Goldreich & Kumar (1988) and Goldreich et al. (1994), successfully used the less efficient dissipation to develop a theory for the damping of the solar  $p$ -modes. In this case the more effective dissipation would require dramatic changes in the excitation mechanism in order to explain the observed amplitudes.

Finally, Goodman & Oh (1997) calculated a lowest order expansion of the effective viscosity, which when applied to Kolmogorov turbulence predicts a

result closer to the less efficient Goldreich & Nicholson viscosity. While this gives a firmer theoretical foundation for the less efficient prescription, it does not help with the observational problem of insufficient dissipation in the case of tides and stellar pulsations.

A possible resolution of this problem is suggested by the fact that the successful applications of the two prescriptions correspond to very different perturbation periods. The Zahn (1966, 1989) scaling seems to work well for periods of order days, and the Goldreich and collaborators quadratic scaling seems to apply to periods of order minutes. This distinction is important, because in stars with surface convection Kolmogorov scaling predicts that the eddies with turnover times of several minutes would have typical sizes that are very small compared to the local pressure scale height and any other external length scales. On the other hand turnover times of days correspond to eddies with typical sizes comparable to, or larger than the local pressure scale height. In this case Kolmogorov scaling is not expected to apply.

The flow seen in 2D and 3D simulations of stellar convection is very different from a Kolmogorov cascade (Sofia & Chan, 1984; Stein & Nordlund, 1989; Malagoli et al., 1990). There are two important distinctions. The first is that the velocity power spectrum is much flatter in the simulations than Kolmogorov, and so one expects to find a slower loss of dissipation efficiency with increased frequency of the external shear, as long as the external shear has a period that corresponds to eddy turnover times too long to fall in the inertial subrange of Kolmogorov turbulence. The second is that the flow is no longer isotropic and hence the effective viscosity should be a tensor, rather than a scalar.

As a first attempt to explore this possibility Penev et al. (2007, 2008b) adapted the Goodman & Oh (1997) perturbative calculation to the Robinson et al. (2003) numerical model of stellar convection and found an asymmetric effective viscosity that scaled linearly with the period of the external shear. However, their perturbative calculation is applicable only as long as the forcing period  $T$  is small compared to the turnover time of the largest eddies. In particular, the perturbative treatment is not able to provide the maximum value the effective viscosity reaches and the frequency at which it reaches it, which is of great importance in calculating tidal interactions and dissipation of pulsations.

In this article we use the Penev et al. (2008a) spectral anelastic code to perform a direct calculation of the turbulent dissipation in a convective zone, by introducing external shear as an extra body force in the fluid equa-

tions. The goal is to investigate the applicability of effective viscosity as an approximation to the actual turbulent dissipation, to derive directly an effective viscosity prescription and compare it against the Goodman & Oh (1997) formalism.

## 2. Simulations

### 2.1. Steady State Convection

The details of the numerical simulation and the equations evolved are presented in Penev et al. (2008a). We are simulating a rectangular box with impenetrable, constant temperature top and bottom boundaries (the  $\hat{z}$  velocity vanishes and the temperature is held at some constant value at the top and bottom walls of the box) using the anelastic approximation. The choice of parameters for our flow and the motivation for this choice is presented in section 4.1 of that article. Here we briefly remind those parameters:

$L_x = L_y = L_z = 4$	physical dimensions of the convective box.
$N_x = N_y = N_z = 128$	resolution in each direction
$p_{top} = 1.0 \times 10^5$	background pressure at the top of the box
$g = 2.74$	gravitational acceleration, in $-\hat{z}$ direction
$C_p = 0.21$	specific heat at constant pressure of the fluid
$R = 8.317 \times 10^{-2}$	ideal gas constant of the fluid
$T_{low} = 10.0$	temperature at the top boundary of the box
$T_{high} = 62.37$	temperature at the bottom boundary of the box

In addition, we need to specify a height dependent heat diffusion coefficient ( $\kappa$ ), which we have plotted in fig. 1.

We initialize the box with random entropy fluctuations and let it evolve with time until a steady state is reached. The criteria we used for concluding a steady state has been reached were that the kinetic and thermal energies should stop drifting systematically, and only exhibit oscillations at the approximate convective turnover time (see fig. 2), and that the spatial spectra of the velocity and potential temperature remain constant to within a few percent. The steady state Fourier spatial and time spectra are presented in fig. 3.

### 2.2. External Forcing

After steady state has been reached we introduce external forcing ( $\mathbf{f}$ ) in the form of a position and time dependent gravitational acceleration in

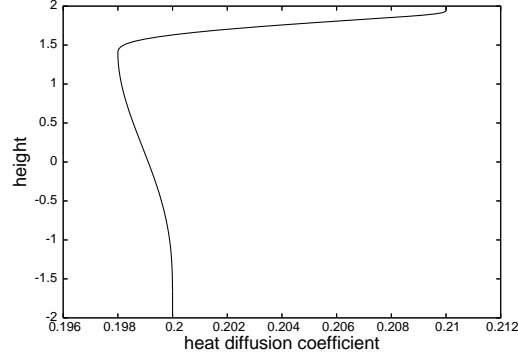


Figure 1: The height dependent heat diffusion coefficient

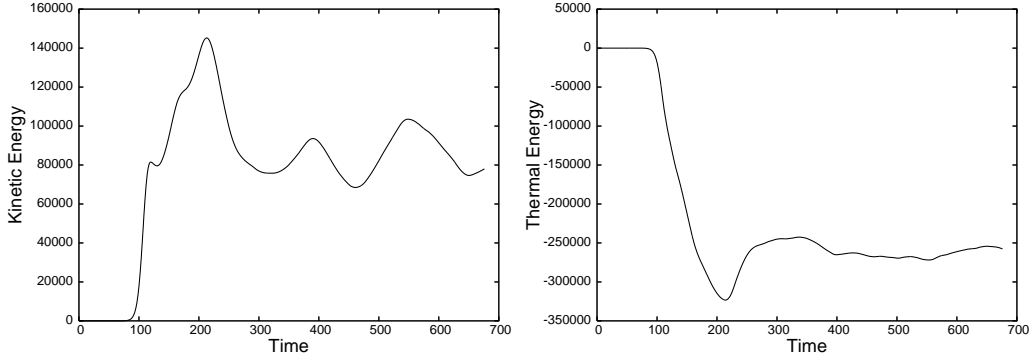


Figure 2: Kinetic (left) and thermal (right) energy content of the convective box used as one of the criteria for having reached a steady state. We decided steady state was reached for times greater than 400.

addition to the already present vertical gravity. So, in short, the anelastic momentum equation that we evolve is:

$$\frac{\partial \mathbf{v}}{\partial t} = \mathbf{v} \times \boldsymbol{\omega} - \nabla \tilde{h} + \frac{\tilde{\theta}}{\bar{\theta}} g \hat{\mathbf{z}} + \mathbf{f} \quad (3)$$

Where quantities with tilde represent anelastic perturbations to the background quantities (denoted by an over bar),  $\mathbf{v}$  is the velocity vector,  $\tilde{h} \equiv \tilde{p}/\bar{\rho} + \mathbf{v}^2/2$  is the enthalpy,  $\tilde{\theta}$  is the perturbation to the background potential temperature,  $\bar{\theta} = \bar{T} (p_0/\bar{p})^{R/C_p}$ , and  $\mathbf{f}$  is the external forcing. We have investigated the effects of two forms of forcing:

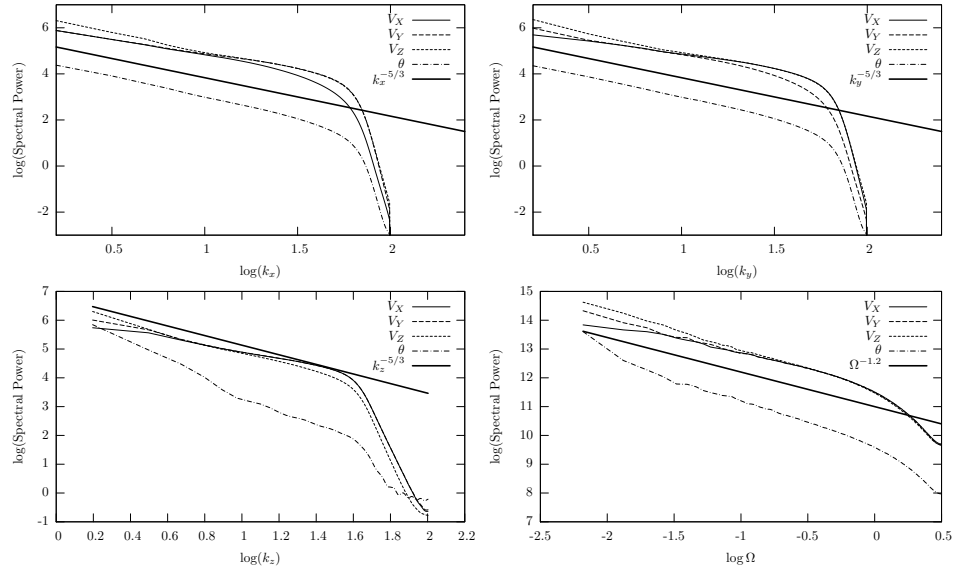


Figure 3: The (x: top left, y: top right, z: bottom left, time: bottom right) spectra of the 3 velocity components and the potential temperature. The thick line in the spatial spectra plots corresponds to Kolmogorov scaling ( $E_k \propto k^{-5/3}$ ). The thick line in the time spectra plot corresponds to the scaling we find for the effective viscosity using the Goodman & Oh (1997) applied on the steady state convection (see eq. 6).

1.  $Z$  (height) dependent horizontal forcing with a Gaussian profile:

$$\mathbf{f}(z, t) = f_0 e^{-2z^2} \cos\left(\frac{2\pi t}{T}\right) \hat{\mathbf{x}} \quad (4)$$

2.  $Y$  dependent forcing in the  $\hat{x}$  direction, again with a Gaussian profile:

$$\mathbf{f}(y) = f_0 e^{-2y^2} \cos\left(\frac{2\pi t}{T}\right) \hat{\mathbf{x}} \quad (5)$$

Clearly the amplitude of the forced velocity will be approximately  $f_0 T / 2\pi$ , so in order to investigate the period dependence of the dissipation, we simulated a number of flows with different periods and the same  $f_0 T$ . That way the shear created by the external forcing was similar for all the flows in the set. We computed two such sets for each forcing case: one with  $f_0 T = 1$  and another with  $f_0 T = 0.15$ . In addition we performed another set of simulations with fixed period and varying values of  $f_0 T$  in order to investigate the effects of the forcing amplitude on the dissipation efficiency. Tables 1, 2 and 3 summarize the runs and the respective number of time steps simulated for each case.

Notice that the weak forcing cases require a lot more time steps in order to average out the turbulent noise and allow us to detect the systematic energy dissipation.

For the strong forcing case we expect the maximal central velocities to reach  $\max v_x = 1/2\pi \approx 0.16$ , and for the weak forcing  $\max v_x = 0.15/2\pi \approx 0.024$ . For comparison in our convective box the speed of sound varies between 1.2 at the top of the box and 2.9 at the bottom and the typical r.m.s. velocity is between 0.02 and 0.04 (see figure 4), except near the boundaries of the box where the collision of the vertical flow with the impenetrable boundaries results in higher horizontal velocities.

In the case of tides in binary stellar systems, the velocities excited by the external forcing are small compared to the typical convective velocities, however, performing numerical simulations with forcing small enough to ensure that this is the case will be prohibitive in terms of computational time, because it will require simulations for excessive number of time steps to make sure the dissipation is noticeable among the fluctuations due to turbulence (see section 3.2).

$$\mathbf{f}(z, t) = f_0 e^{-2z^2} \cos\left(\frac{2\pi t}{T}\right) \hat{\mathbf{x}}$$

<b>Strong Forcing</b>				<b>Weak Forcing</b>			
$T$	$f_0$	number time steps	saving one time step out of every	$T$	$f_0$	number time steps	saving one time step out of every
300	1/300	120000	10	200	0.15/200	420000	10
250	1/250	150000	10	150	0.15/150	300000	50
225	1/225	135000	10	140	0.15/140	168000	10
200	1/200	60000	10	120	0.15/120	240000	10
190	1/190	133000	10	110	0.15/110	220000	10
180	1/180	144000	10	100	0.15/100	180000	10
170	1/170	136000	10	90	0.15/90	189000	10
160	1/160	144000	10	75	0.15/75	225000	10
150	1/150	60000	50	60	0.15/60	186000	10
140	1/140	126000	10	50	0.15/50	190000	50
120	1/120	60000	10	30	0.15/30	171000	10
110	1/110	66000	10				
105	1/105	73500	10				
100	1/100	60000	50				
95	1/95	57000	10				
90	1/90	63000	10				
80	1/80	112000	10				
75	1/75	45000	50				
70	1/70	63000	10				
60	1/60	60000	10				
55	1/55	60500	10				
50	1/50	60000	50				
45	1/45	63000	10				
40	1/40	60000	10				
30	1/30	63000	50				
10	1/10	60000	50				

Table 1: The forcing amplitude–period combinations for the simulations with constant amplitude and variable period  $z$  dependent  $x$  forcing, along with the number of time steps simulated in each case.



$$\mathbf{f}(y, t) = f_0 e^{-2y^2} \cos\left(\frac{2\pi t}{T}\right) \hat{\mathbf{x}}$$

<b>Strong Forcing</b>				<b>Weak Forcing</b>			
$T$	$f_0$	number time steps	saving one time step out of every	$T$	$f_0$	number time steps	saving one time step out of every
300	1/300	300000	10	290	0.15/290	580000	10
290	1/290	319000	10	270	0.15/270	540000	10
270	1/270	270000	10	250	0.15/250	525000	10
250	1/250	250000	10	230	0.15/230	460000	10
230	1/230	230000	10	210	0.15/210	420000	10
210	1/210	273000	10	190	0.15/190	399000	10
190	1/190	?????	10	170	0.15/170	340000	10
170	1/170	136000	10	150	0.15/150	300000	10
150	1/150	225000	10	130	0.15/130	260000	10
130	1/130	143000	10	110	0.15/110	231000	10
110	1/110	143000	10	100	0.15/100	360000	10
90	1/90	144000	10	90	0.15/90	270000	10
70	1/70	84000	10	80	0.15/80	344000	10
50	1/50	60000	10	70	0.15/70	238000	10
30	1/30	145000	10	60	0.15/60	270000	10
				50	0.15/50	200000	10
				40	0.15/40	344000	10
				30	0.15/30	150000	10

Table 2: The forcing amplitude–period combinations for the simulations with constant amplitude and variable period  $y$  dependent  $x$  forcing, together with number of time steps simulated in each case.

$$\mathbf{f}(z, t) = f_0 e^{-2z^2} \cos\left(\frac{2\pi t}{T}\right) \hat{\mathbf{x}}$$

$T$	$f_0$	number time steps	saving one time step out of every
50	0.8/50	515000	10
50	0.6/50	500000	10
50	0.4/50	500000	10
50	0.2/50	500000	10

Table 3: The forcing amplitude–period combinations for the simulations with constant period and variable amplitude  $z$  dependent  $x$  forcing, together with the number of time steps simulated in each case.

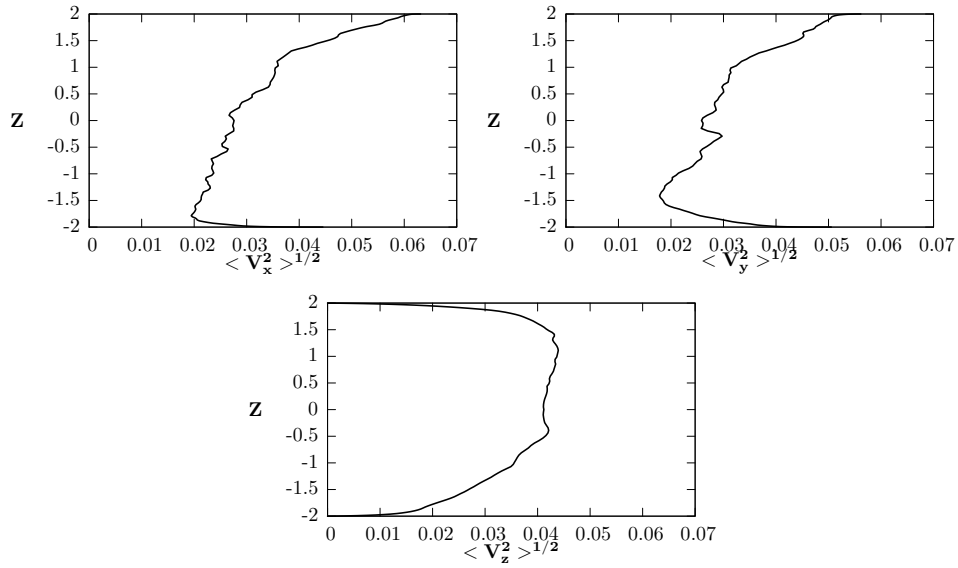


Figure 4: The typical steady state r.m.s. velocities ( $v_x$  top left,  $v_y$  top right,  $v_z$  bottom).

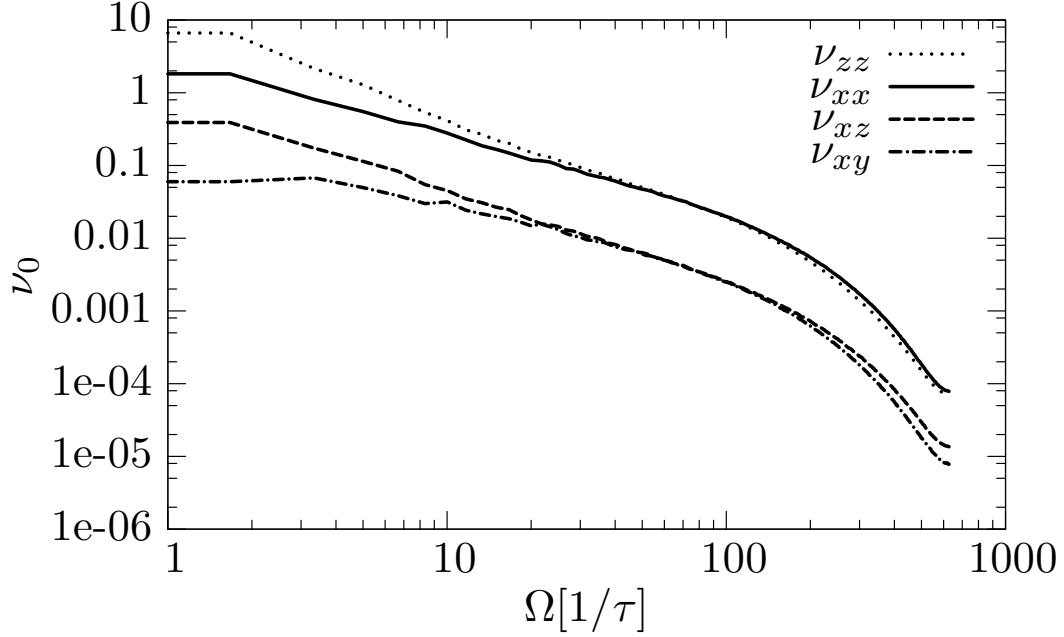


Figure 5: The four independent components of the viscosity tensor estimated using the perturbative approach of Goodman & Oh (1997).

### 3. Results

#### 3.1. Perturbative Calculation

The obvious first step is to apply the Goodman & Oh (1997) perturbative calculation, as modified in Penev et al. (2007) and Penev et al. (2008b) to account for density stratification and discretely sampled data, to the steady state flow without any forcing. The details of that calculation were presented in Penev et al. (2008a) section 5.2. We include here again the components of the effective viscosity tensor this calculation predicts in figure 5. The figure contains only four curves (rather than nine), since by assumption the viscosity tensor produced by this method is symmetric, and also physically we expect no difference between the  $\hat{x}$  direction and the  $\hat{y}$  direction in our simulations, so we average the corresponding viscosity components together and only four independent components remain.

The approximate scaling with frequency of the volume average effective

viscosity we observe is roughly the same for all four components:

$$\nu \propto \Omega^{-1.2 \pm 0.1} \quad (6)$$

### 3.2. Direct Calculation

To simplify the discussion we define upfront the following quantities for the  $z$  dependent forcing:

$$C_{xz}(z) = \sum_{i,j,w} v_x(x_i, y_j, z, t_w) \cos\left(\frac{2\pi t_w}{T}\right) \quad (7)$$

$$S_{xz}(z) = \sum_{i,j,w} v_x(x_i, y_j, z, t_w) \sin\left(\frac{2\pi t_w}{T}\right) \quad (8)$$

and for the  $y$  dependent forcing:

$$C_{xy}(y, z) = \sum_{i,j,w} v_x(x_i, y, z, t_w) \cos\left(\frac{2\pi t_w}{T}\right) \quad (9)$$

$$S_{xy}(y, z) = \sum_{i,j,w} v_x(x_i, y, z, t_w) \sin\left(\frac{2\pi t_w}{T}\right) \quad (10)$$

Where  $x_i$  and  $y_j$  are the locations of the  $x$  and  $y$  collocation grid points where we have values for the velocity and  $t_w$  are the times at which we have them. We evaluate the sum over an integer number of forcing periods  $T$ .

#### 3.2.1. Depth Dependence of the Effective Viscosity

We use pre-determined functions of depth up to a normalization constant for the effective viscosity coefficients that we need. namely:

$$\nu_{xz} = \nu_{xz}^0 \langle v_z^2 \rangle^{1/2} H_p \quad (11)$$

$$\nu_{xy} = \nu_{xy}^0 \left\langle \frac{v_x^2 + v_y^2}{2} \right\rangle^{1/2} H_p \quad (12)$$

Where  $H_p$  is the pressure scale height. This way we have only one free parameter for each viscosity component:  $\nu_{xz}^0$  or  $\nu_{xy}^0$ . On dimensional grounds the turbulent viscosity must scale like the relevant velocity and length scales in the problem. Clearly the relevant velocity scale is the convective velocity and it seems reasonable to use the velocity in the direction of the shear. In equation 12 we average together both horizontal components of the velocity

because there is no physical difference between the two. We use  $H_p$  as the length scale in keeping with mixing length theory, where it is assumed that the mixing length will be proportional to the local pressure scale height. One could argue that we should then include the mixing length parameter ( $\alpha$ ), but that simply gets absorbed into the definition of the  $\nu_{xz}^0$  and  $\nu_{xy}^0$  coefficients, and we note that it is reasonable to expect that the values of  $\nu_{xz}^0$  and  $\nu_{xy}^0$  will scale as the mixing length parameter of the convective region. In fact this is seen to be the case by comparing our perturbative calculation results to those of Penev et al. (2008b) (see sec. 4).

A slightly modified version of equations 11 and 12 ( $\nu \propto 1/3 < v^2 >^{1/2} H_p$ ) has been assumed in all previous effective viscosity applications (Zahn, 1966, 1989; Goldreich & Keeley, 1977; Goldreich & Kumar, 1988; Goldreich et al., 1994). Those works assumed that the effective viscosity and the underlying turbulent velocity field is isotropic, so there was no need to consider different components of the velocity separately. In practice this distinction makes little difference since as we can see from fig. 4 away from the boundaries all components of the velocity behave alike, except for the fact that  $v_z$  tends to be larger. So, using the full r.m.s. velocity instead of only one component, just leads to smaller values of the normalization constants  $\nu_{xz}^0$  and  $\nu_{xy}^0$ .

### 3.2.2. Fitting the Spatial Dependence of the Dissipation

We would like to explore the applicability of the effective viscosity framework to the problem of turbulent dissipation. We would like to show that substituting the turbulent flow with a simple viscosity is able to capture not only the total amount of energy dissipated, but also the momentum transport or in other words the spatial dependence of this dissipation.

For the  $z$  dependent  $x$  forcing we would like to show that the work per unit mass done by the forcing on the flow at each depth:

$$W_{xz}^{turb}(z) \equiv f_0 e^{-2z^2} C_{xz}(z) \quad (13)$$

matches the energy that would be transported and dissipated out of that depth by an assumed effective viscosity:

$$\begin{aligned} W_{xz}^{visc}(z) \equiv & \nu_{xz}(z) [C_{xz}(z)C_{xz}''(z) + S_{xz}(z)S_{xz}''(z)] + \\ & + \left( \nu'_{xz}(z) + \frac{d \log \bar{\rho}}{dz} \nu(z) \right) [C_{xz}(z)C_{xz}'(z) + S_{xz}(z)S_{xz}'(z)] \end{aligned} \quad (14)$$

Where primes denote derivatives with respect to  $z$  and  $\bar{\rho}$  is the background density profile.

For the  $y$  dependent  $x$  forcing we would like to show that the work per unit mass done by the forcing on the flow at each  $y$  plane:

$$W_{xy}^{turb}(y) \equiv \frac{f_0}{N} e^{-2y^2} \int_{z_{min}}^{z_{max}} \bar{\rho}(z) C_{xy}(y, z) dz \quad (15)$$

matches the energy that would be transported and dissipated out of that plane by an assumed effective viscosity:

$$W_{xy}^{visc}(y) \equiv \frac{1}{N} \int_{z_{min}}^{z_{max}} \bar{\rho}(z) \nu_{xy}(z) \left[ C_{xy}(y, z) C_{xy}''(y, z) + S_{xy}(y, z) S_{xy}''(y, z) \right] dz \quad (16)$$

Where now primes denote derivatives with respect to  $y$ ,  $z_{min}$  and  $z_{max}$  are the minimal and maximal depth respectively that we want to include in the fit and  $N \equiv \int_{z_{min}}^{z_{max}} \bar{\rho}(z) dz$ . The reason we do not want to include the entire simulated domain is that near the boundaries the flow is strongly affected by the impenetrable top and bottom walls and is thus non-physical.

We find the values of  $\nu_{xz}^0$  and  $\nu_{xy}^0$  by least squares fitting of  $W_{xz}^{visc}$  to  $W_{xz}^{turb}$  in the range  $z_{min} < z < z_{max}$  and  $W_{xy}^{visc}$  to  $W_{xy}^{turb}$  in the range  $-L_y/2 < y < L_y/2$  respectively. Clearly the presence of the turbulence will cause random fluctuations in the velocity profile which should average out if we combine a large enough number of time steps in evaluating the quantities  $C_{xz}$ ,  $C_{xy}$ ,  $S_{xz}$  and  $S_{xy}$ . These fluctuations are highly amplified when we estimate second derivatives of those quantities, so  $W_{xz}^{visc}$  and  $W_{xy}^{visc}$  suffer much more than  $W_{xz}^{turb}$  and  $W_{xy}^{turb}$ . Some representative fitted curves for each series of runs are shown in figures 6, 7 and 8.

We see that, except for one case, the two curves match closely which shows that the effective viscosity assumption captures the effects of turbulent dissipation to a good degree. The  $T = 10$  curves for the strong  $z$  dependent  $x$  forcing case do not match well at all. The bad fit is due to the fact that if there is any dissipation present it is undetectable from within the turbulent noise. The reason for the strongly suppressed dissipation is that for such short periods the corresponding eddy size is too small to be reliably simulated at our current resolution.

### 3.2.3. Matching Deposited to Dissipated Power

An alternative way to get a value for the scaling constants  $\nu_{xz}^0$  and  $\nu_{xy}^0$  is to equate the overall power deposited into the box by the external forcing:

$$\dot{\epsilon}_{xz}^{ext} = \int_{-z_{min}}^{z_{max}} \bar{\rho}(z) W_{xz}^{turb}(z) dz \quad \text{for} \quad \nu_{xz}^0 \quad (17)$$

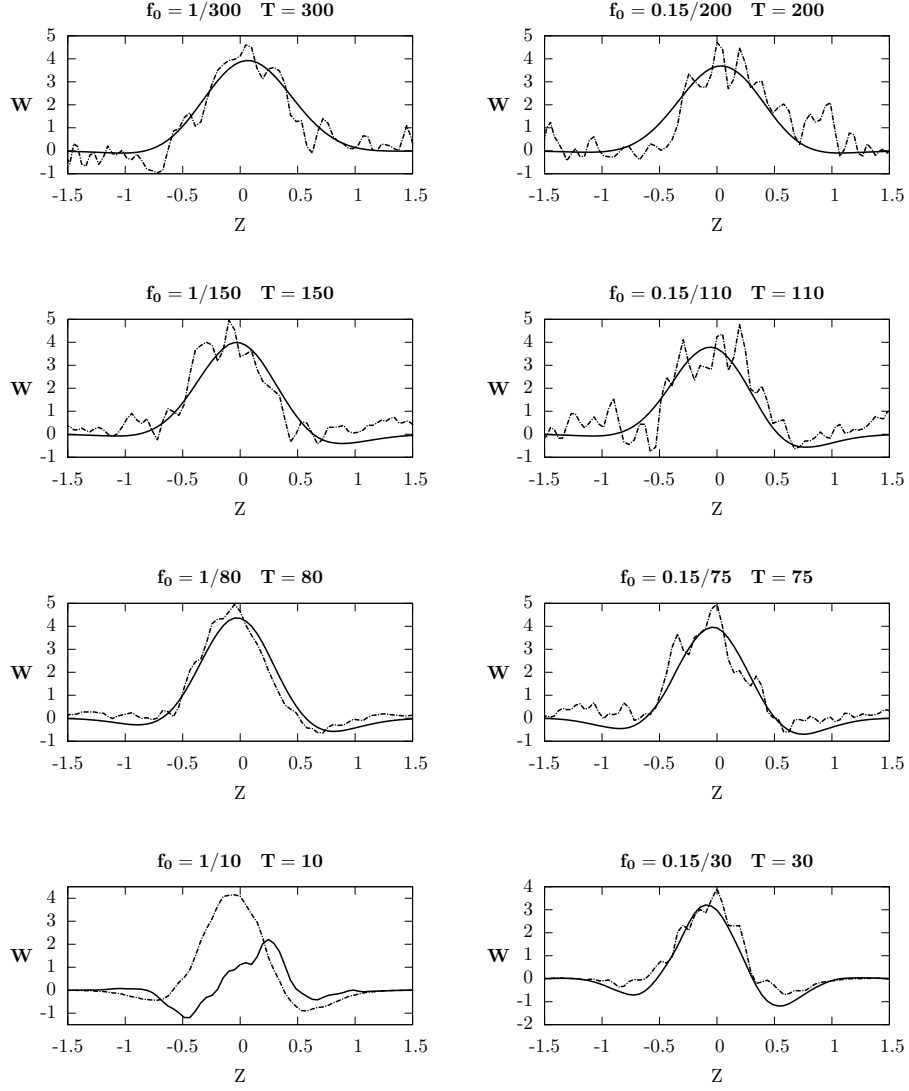


Figure 6: Typical least squares fits between  $W_{xz}^{turb}$  (solid curves) and  $W_{xz}^{visc}$  (dashed curves) for the two sets of simulations with  $z$  dependent  $x$  forcing with fixed amplitude and variable period. Left: strong forcing, right: weak forcing. In each plot  $W_{xz}^{turb}$  and  $W_{xz}^{visc}$  have been scaled in order to make their maximum values be of order few.

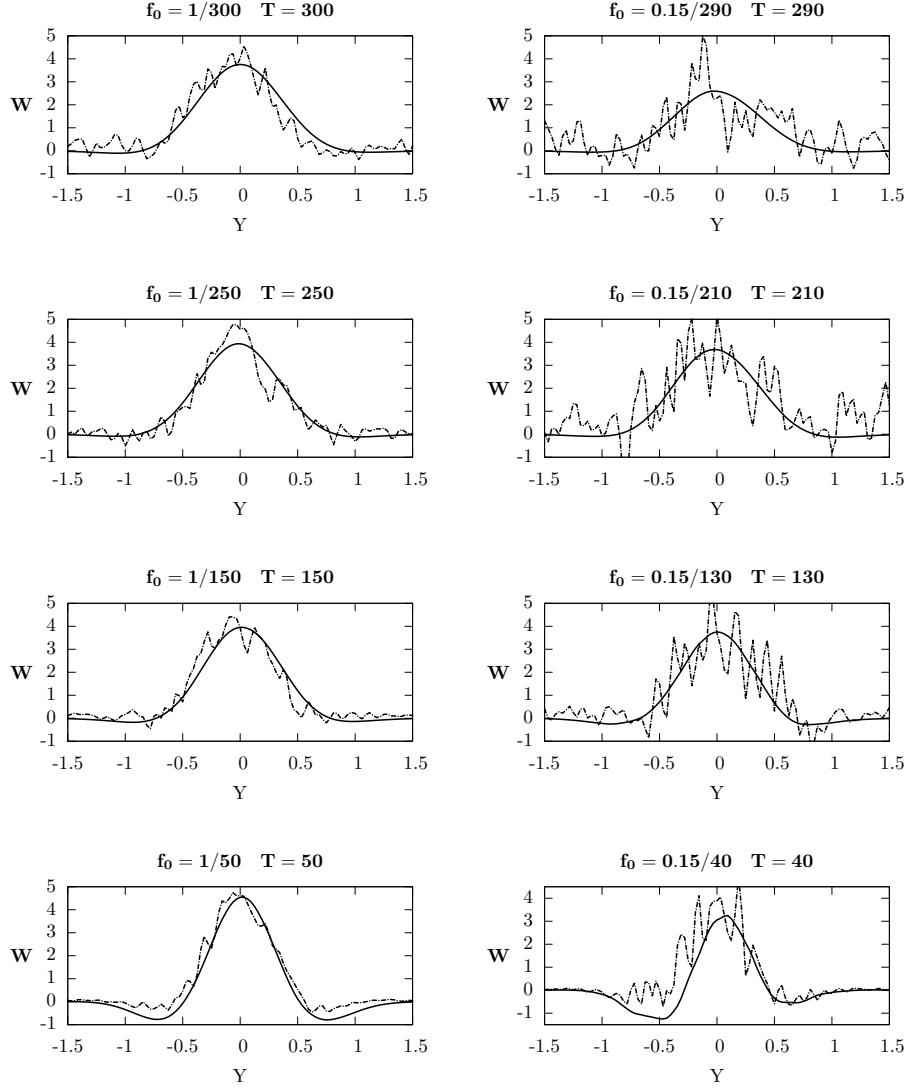


Figure 7: Typical least squares fits between  $W_{xy}^{turb}$  (solid curves) and  $W_{xy}^{visc}$  (dashed curves) for the two sets of simulations with  $y$  dependent  $x$  forcing with fixed amplitude and variable period. Left: strong forcing, right: weak forcing. In each plot  $W_{xy}^{turb}$  and  $W_{xy}^{visc}$  have been scaled in order to make their maximum values be of order few.



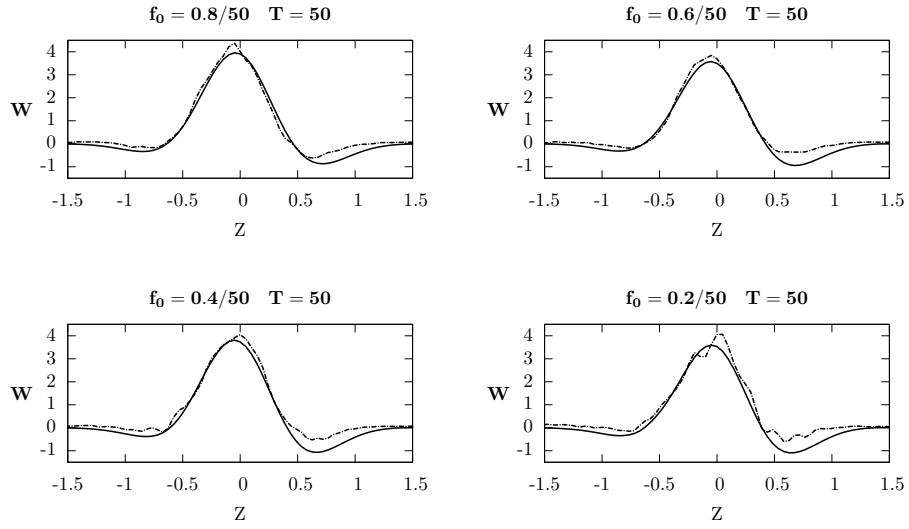


Figure 8: The least squares fits between  $W_{xz}^{turb}$  (solid curves) and  $W_{xz}^{visc}$  (dashed curves) for the set of simulations with  $z$  dependent  $x$  forcing with fixed period and variable amplitude. In each plot  $W_{xz}^{turb}$  and  $W_{xz}^{visc}$  have been scaled in order to make their maximum values be of order few.

$$\dot{\varepsilon}_{xy}^{ext} = N \int_{-Ly/2}^{Ly/2} W_{xy}^{turb}(y) dy \quad \text{for} \quad \nu_{xy}^0 \quad (18)$$

to the value that the effective viscosity dissipates out of the box:

$$\dot{\varepsilon}_{xz}^{visc} = \int_{-z_{min}}^{z_{max}} \bar{\rho}(z) \widetilde{W}_{xz}^{visc}(z) dz \quad \text{for} \quad \nu_{xz}^0 \quad (19)$$

$$\dot{\varepsilon}_{xy}^{visc} = \int_{-Ly/2}^{Ly/2} \widetilde{W}_{xy}^{visc}(y) dy \quad \text{for} \quad \nu_{xy}^0 \quad (20)$$

Where we have defined:

$$\widetilde{W}_{xz}^{visc}(z) \equiv \nu(z) \left[ \left( \frac{dC_{xz}}{dz} \right)^2 + \left( \frac{dS_{xz}}{dz} \right)^2 + \right] \quad (21)$$

$$\widetilde{W}_{xy}^{visc}(y) \equiv \int_{z_{min}}^{z_{max}} \bar{\rho}(z) \nu(z) \left[ \left( \frac{\partial C_{xy}}{\partial y} \right)^2 + \left( \frac{\partial S_{xy}}{\partial y} \right)^2 \right] dz \quad (22)$$

Note that in this case we do not expect to match the spatial dependence, only the overall rate. The reason for this is that viscous forces redistribute the energy in the box as well as dissipate it. So we cannot use these quantities to examine the applicability of the effective viscosity assumption.

Because evaluating  $\widetilde{W}_{xz}^{visc}(z)$  and  $\widetilde{W}_{xy}^{visc}(y)$  requires only first derivatives of the sin and cos velocity components they suffer significantly less from the turbulent noise than  $W_{xz}^{visc}(z)$  and  $W_{xy}^{visc}(y)$  from section 3.2.2. On the other hand some energy transfer inevitably occurs near the top and bottom boundaries, which is excluded from evaluating the  $z$  integrals. For the case of  $z$  dependent forcing this is a very small quantity since the forcing in that part of the box is very small by design. However, for the  $y$  dependent forcing significant energy transfer does occur in those regions, which could bias the estimated viscosities toward lower values (see the last paragraph of section 3.3).

Plots of  $\widetilde{W}_{xz}^{visc}(z)$  and  $\widetilde{W}_{xy}^{visc}(y)$  for the same cases as in figures 6, 7 and 8 are shown in figures 9, 10 and 11 respectively, where we have taken  $z_{max} = -z_{min} = 1.5$  for the depth dependent forcing and  $z_{max} = -z_{min} = 1.8$  for the  $y$  dependent forcing.

### 3.3. Comparison Between the Perturbative and Direct Calculation

We compare the Goodman & Oh (1997) based perturbative estimate of the  $\nu_{xz}$  and  $\nu_{xy}$  viscosity coefficients to the directly calculated effective viscosity obtained by the procedures of sec. 3.2.2 and 3.2.3 in figures 12 and 13.

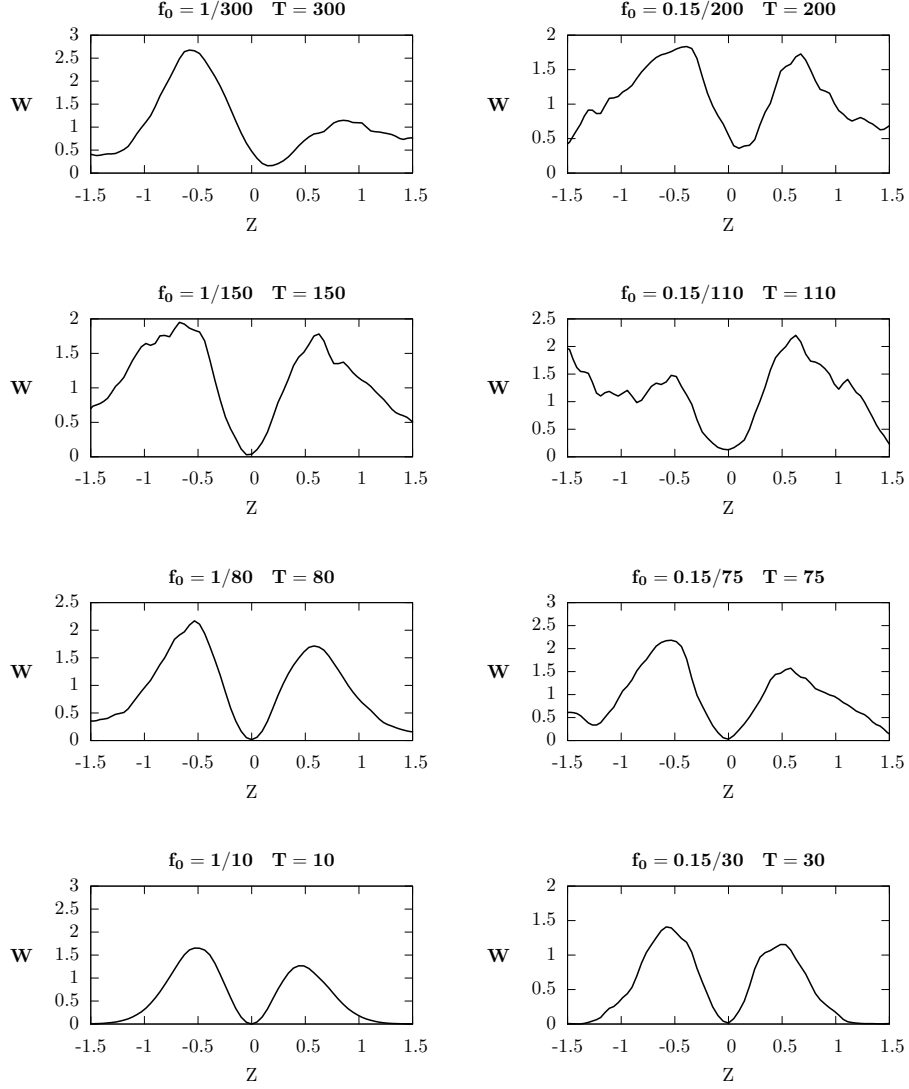


Figure 9: The energy dissipation rate due to the effective viscosity at each depth for the two sets of simulations with  $z$  dependent  $x$  forcing with fixed amplitude and variable period. Left: strong forcing, right: weak forcing. The plots are for the same simulations as the plots in figure 6. The same scaling has been applied to each plot as in figure 6

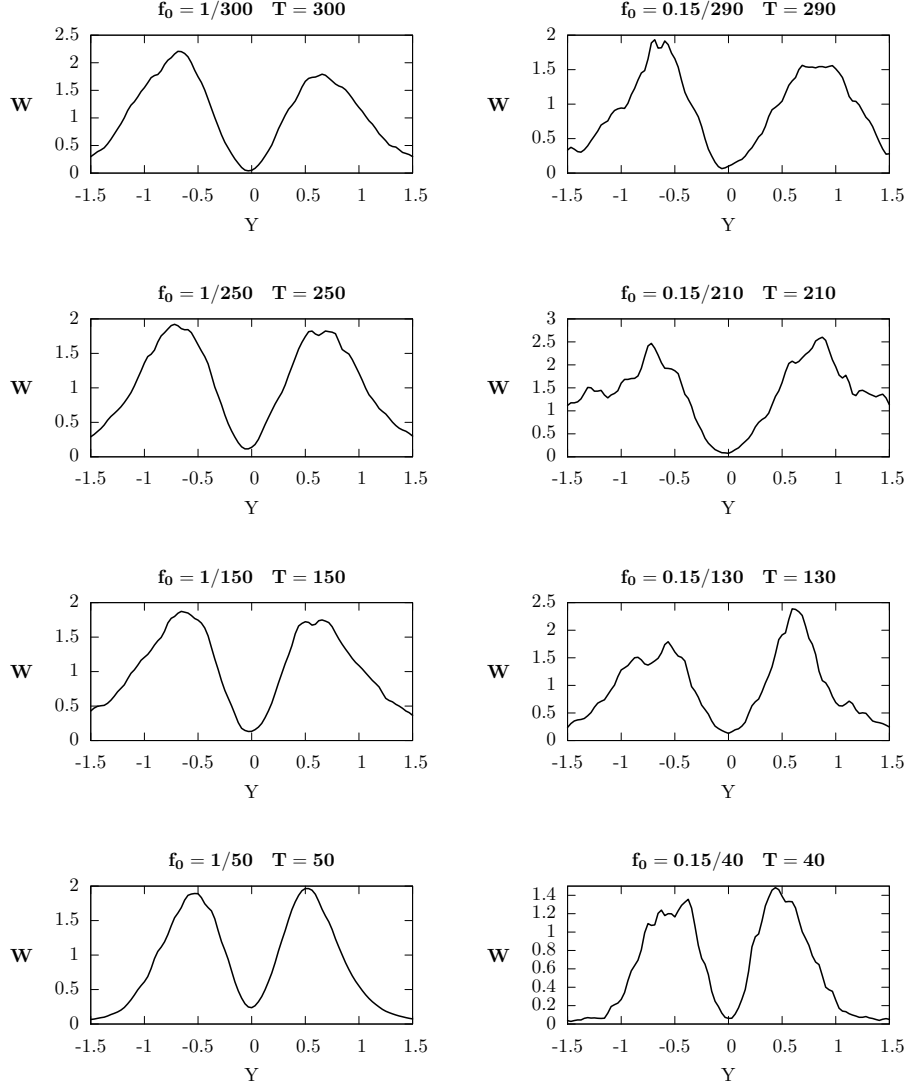


Figure 10: The energy dissipation rate due to the effective viscosity at each depth for the two sets of simulations with  $y$  dependent  $x$  forcing with fixed amplitude and variable period. Left: strong forcing, right: weak forcing. The plots are for the same simulations as the plots in figure 7. The same scaling has been applied to each plot as in figure 6

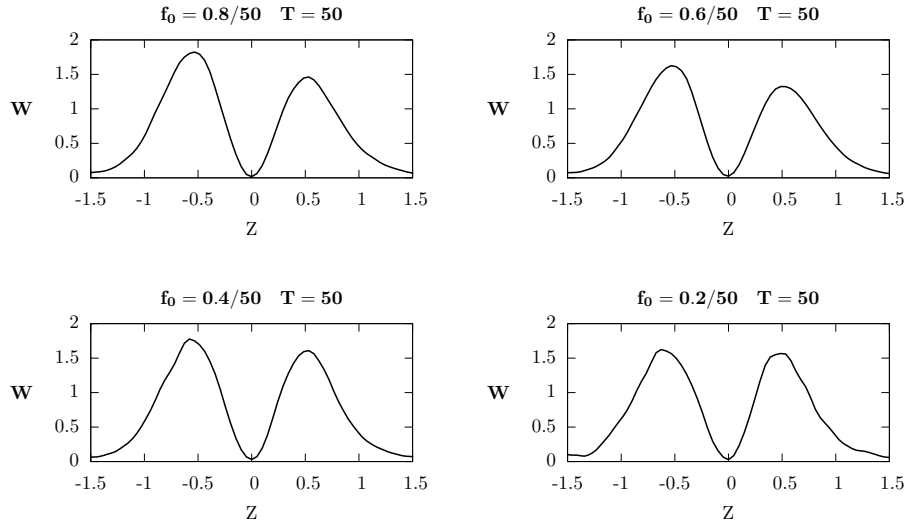


Figure 11: The energy dissipation rate due to the effective viscosity at each depth for the two sets of simulations with  $y$  dependent  $x$  forcing with fixed period and variable amplitude. The plots are for the same simulations as the plots in figure 8. The same scaling has been applied to each plot as in figure 6

The curves in those figures correspond to the perturbative expansion, and the points correspond to the direct calculation. Since the perturbative calculation assumes that the forcing period is small compared to the convective turnover time we have used a solid line only for  $T < \tau$ . For longer periods (dotted line) this method is no longer applicable.

We see that the effective viscosity predicted with all three methods scales linearly with the forcing period for most of the range covered by our simulations. Further, the direct calculations with strong forcing show that the  $x-z$  component of the effective viscosity saturates at  $T \approx 2.2\tau$ , after which it remains roughly constant. One physically expects to see this saturation, because for forcing periods much larger than any convective timescales there is no reason why the dissipation efficiency of the convective zone should depend on the period.

We do not see the saturation in the weak forcing case, because there are no points at long enough perturbation periods. The reason for this is that longer forcing period simulations require more time steps in order to achieve acceptable fits, hence they become very time consuming to compute in the weak forcing case. We also do not see the saturation for the perturbative calculation, because it is due to the neglected higher order terms. No obvious saturation is present for  $\nu_{xy}^0$  either. This could be simply because we do not have enough long period points to see it, or it could mean that the saturation occurs at longer period than for  $\nu_{xz}^0$ .

In order to obtain a functional dependence for the effective viscosity on period we perform a least square fit to the direct calculation points, where we fit a linear function for all cases except the strong  $z$  dependent forcing, where we allow for saturation. The resulting fits are shown in figures 12 and 13 as solid lines for the weak forcing cases and dashed lines for the strong forcing cases. The linear fits for  $\nu_{xy}^0$  are based only on the points with  $P < 1.5\tau$  in order to avoid including points which are possibly starting to saturate. The parameters of the fitted lines are given in tables 4 and 5. This also allows us to get an estimate of the error bars associated with the points. Those are shown in the upper left corners of the plots in figures 12 and 13.

Since for very short periods the perturbative calculation should be valid, and the turbulence should be well approximated by a Kolmogorov cascade we expect that the scaling of the effective viscosity with period should be quadratic for those short periods. This means that we expect to see positive zero crossings of the best fit linear approximations to the effective viscosity. From tables 4 and 5 we see that this is indeed the case except for the dissipa-

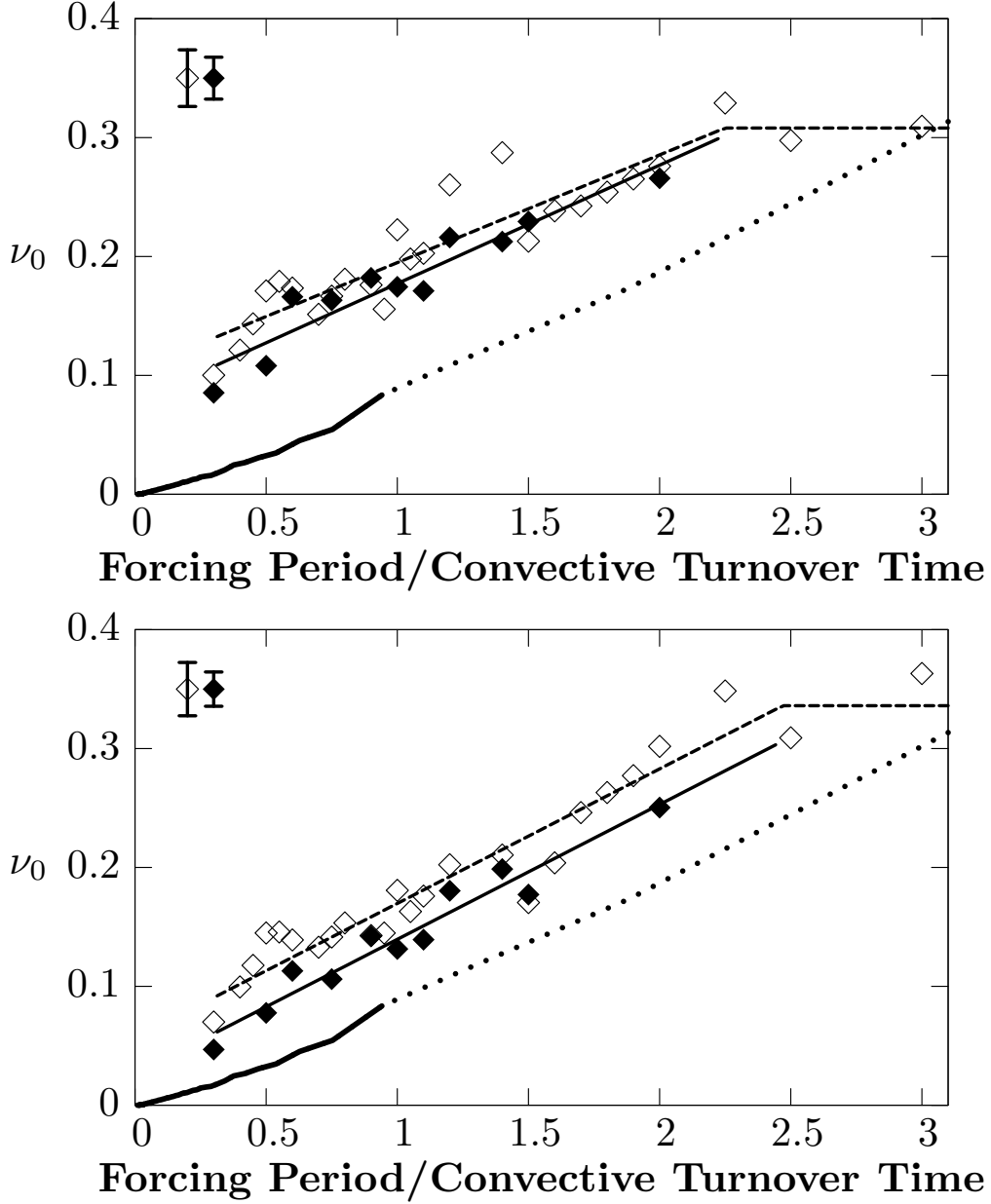


Figure 12: Comparison between the after-the-fact perturbatively estimated  $\nu_{xz}^0$  (curve) and the viscosity obtained from the direct simulations by least squares fit of  $\widetilde{W}_{xz}^{visc}$  (eq. 15) to  $W_{xz}^{turb}$  (eq. 13) — top ; and from setting  $\int W_{xz}^{turb}(z) = \int \widetilde{W}_{xz}^{visc}(z)$  — bottom. The strong forcing points are plotted with empty symbols, and the weak forcing with filled symbols. The horizontal axis is the perturbation period ( $T$ ) in units of the convective turnover time in the box and the vertical axis is the value of the scaling constant  $\nu_0$  (eq. 11). Also shown are linear least square fits to the strong forcing points (dashed line) and the weak forcing points (solid line) as well as an estimate of the maximum effective viscosity for the strong forcing case. The error bars top left corner of the plots correspond to the standard deviation of  $\nu_{xz}^0$  (assumed the same for all points) obtained from the differences with the fitted curves.

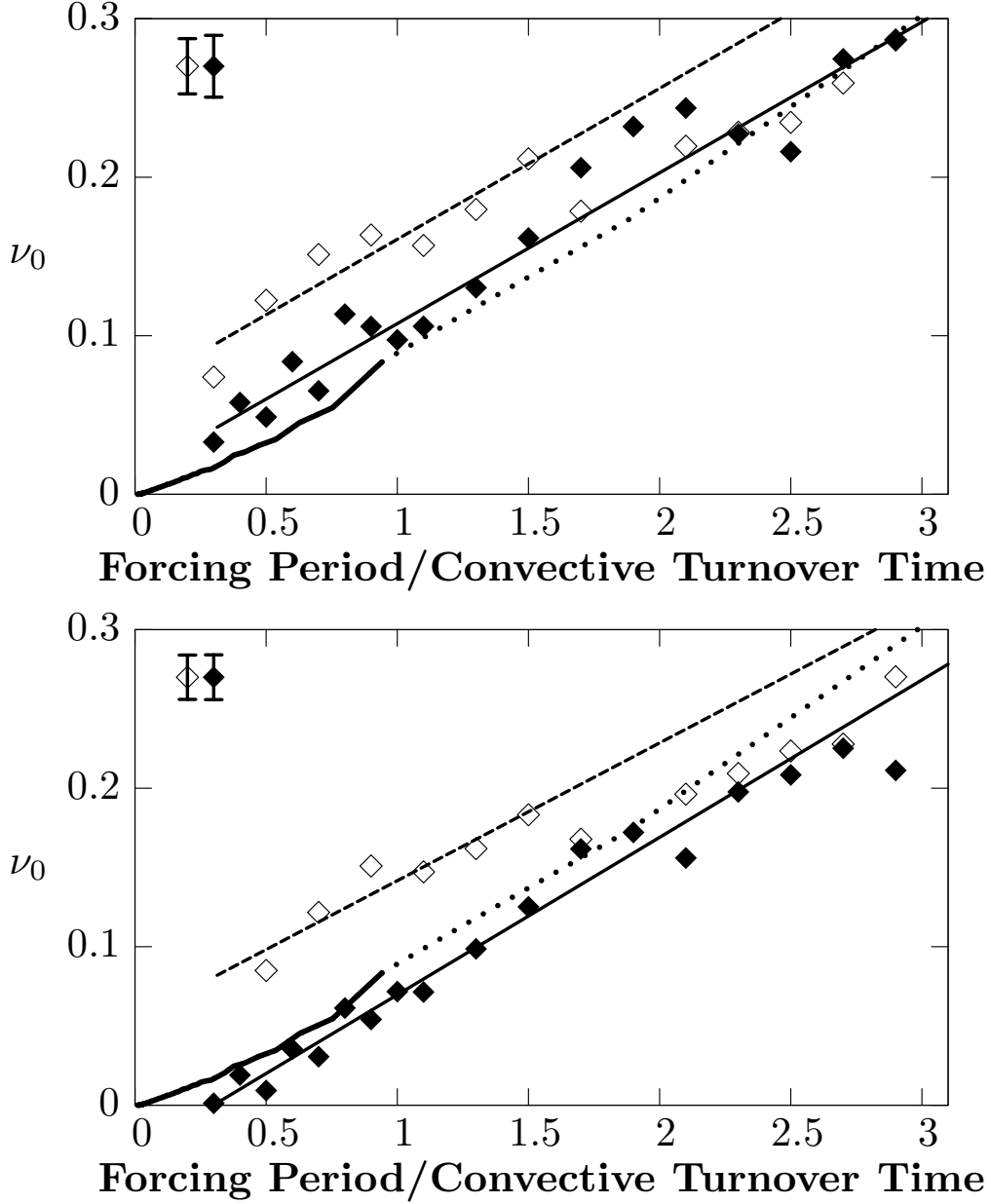


Figure 13: Comparison between the after-the-fact perturbatively estimated  $\nu_{xy}^0$  (curve) and the viscosity obtained from the direct simulations by least squares fit of  $W_{xy}^{visc}$  (eq. 16) to  $W_{xy}^{turb}$  (eq. 15) — top ; and from setting  $\int W_{xy}^{turb}(z) = \int \widetilde{W}_{xy}^{visc}(z)$  — bottom. The strong forcing points are plotted with empty symbols, and the weak forcing with filled symbols. The horizontal axis is the perturbation period ( $T$ ) in units of the convective turnover time in the box and the vertical axis is the value of the scaling constant  $\nu_{xy}^0$  (eq. 12). Also shown are linear least square fits to the strong forcing points (dashed line) and the weak forcing points (solid line). The error bars top left corner of the plots correspond to the standard deviation of  $\nu_{xy}^0$  (assumed the same for all points) obtained from the differences with the fitted curves.



	Depth Fit (sec. 3.2.2)		Dissipation Match (sec. 3.2.3)	
	slope	zero intercept	slope	zero intercept
strong forcing	$0.090 \pm 0.009$	$0.104 \pm 0.011$	$0.113 \pm 0.008$	$0.057 \pm 0.010$
weak forcing	$0.100 \pm 0.011$	$0.078 \pm 0.013$	$0.113 \pm 0.009$	$0.026 \pm 0.010$

Table 4: The linear regression parameters corresponding to the solid and dashed lines in fig. 12.

	Y Fit (sec. 3.2.2)		Dissipation Match (sec. 3.2.3)	
	slope	zero intercept	slope	zero intercept
strong forcing	$0.064 \pm 0.006$	$0.088 \pm 0.010$	$0.078 \pm 0.012$	$0.039 \pm 0.021$
weak forcing	$0.096 \pm 0.006$	$0.015 \pm 0.009$	$0.091 \pm 0.004$	$-0.021 \pm 0.007$

Table 5: The linear regression parameters corresponding to the solid and dashed lines in fig. 13.

tion matching estimate of  $\nu_{xy}^0$  for weak forcing. We believe that this negative zero crossing is caused by the fact that the forcing in this case is not small near the boundaries and as a result significant energy is deposited there by the external forcing, especially since in those regions the horizontal velocity is very large, due to the collision of the mainly vertical flow in the bulk of the box with the impenetrable boundaries. This large horizontal flow is non physical and as such we do not include the regions near the boundaries in our calculations. Ignoring this external energy source is not important for the fitting of the spatial dependence of the deposited energy since it will be ignored from both  $W_{xy}^{turb}$  and  $W_{xy}^{visc}$ . However, if some amount of this energy makes it to the region of the box used to calculate  $\widetilde{W}_{xy}^{visc}$  before the turbulent cascade has dissipated it it will act to artificially increase  $\widetilde{W}_{xy}^{visc}$ , and consequently decrease the effective viscosity we calculate.

### 3.3.1. Amplitude Dependence

The three dependences in each of the plots of figures 12 and 13 correspond to three different forcing strengths: strong forcing with  $v_{forc}/v_{conv} \approx 2.7$ , weak forcing with  $v_{forc}/v_{conv} \approx 0.4$  and the perturbative calculation with  $v_{forc}/v_{conv} \ll 1$ , where  $v_{forc}$  is the peak velocity due to the external forcing and  $v_{conv}$  is the root mean square velocity for the central plane of the box in the absence of forcing.

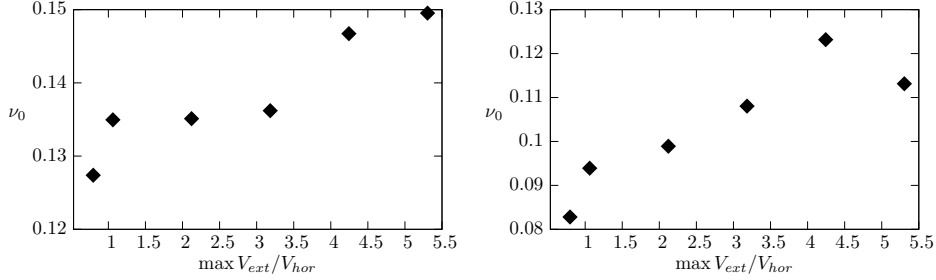


Figure 14: The dependence of the effective viscosity  $\nu_{xz}^0$  on the forcing strength ( $\max V_{ext}/V_{hor}$ ), where  $V_{hor}$  is the horizontal r.m.s. velocity in the absence of forcing. The left plot correspond to the effective viscosity estimated by least squares fitting of  $W_{xz}^{visc}$  (eq. 15) to  $W_{xz}^{turb}$  (eq. 13) and the right plot corresponds to the effective viscosity obtained by setting  $\int W_{xz}^{turb}(z) = \int \widetilde{W}_{xz}^{visc}(z)$

The systematic differences between each set of viscosities suggest a possibly important amplitude dependence of the dissipation efficiency. In order to get some idea for the importance of the magnitude of the external shear in determining the values of  $\nu_{xz}^0$  we performed four additional simulations with  $z$  dependent external forcing with period  $T = \tau/2$  with strengths intermediate between the strong and weak forcing cases considered above (see table 3 for the details of each run and figures 8 and 11 for the energy rate curves). Using the same two methods discussed above, we estimate the effective viscosity for those cases, which we plot in figure 14 where we have also added the value of the fitted straight lines for the strong and weak forcing from figure 12 at half the convective turnover time.

Clearly the effective viscosity increases for larger external forcing, but the effect is relatively much smaller than the period dependence. Further, the perturbative calculation, which would correspond to a forcing strength of zero has a value at  $T = \tau/2$  of 0.03, which is much smaller than the direct calculation values obtained from either method. This is possibly due to the fact that at the periods covered by our direct calculation points the value of  $T/\tau$  is not small enough for the perturbative calculation to be a good approximation. Another possibility is that for weaker forcings the amplitude dependence is much stronger, but we must note that according to the perturbative calculation for very small amplitudes the effective viscosity is independent of the amplitude of the external shear.

From figure 13 we see that this discrepancy between the direct calculation

and the perturbative calculation does not exist for  $\nu_{xy}^0$  and the weak forcing direct calculation points lie close to the the perturbative calculation curve.

#### 4. Conclusions

We have completed a set of simulations of turbulent convection relevant to stellar surface convective zones with external forcing introduced directly in the momentum equation, in the form of a periodic, horizontal, position dependent gravitational acceleration. We then found an effective viscosity assumed to be of the form of equations 11 and 12 (in accordance with mixing length theory), using two methods:

1. least squares fitting of the work done by the external forcing on the flow at each  $z$  or  $y$  grid plane respectively to the energy transported or dissipated away from that plane by the effective viscosity.
2. matching the overall energy deposited into the box by the external forcing to the energy dissipated by the effective viscosity.

Both methods produce effective viscosity that scales linearly with period with the same slope, and the two methods differ by a constant offset. Further, we found that the one parameter fits of the first method were able to capture the details of the observed position dependence of the deposited energy (see fig. 9, 10 and 11), which suggests that the effective viscosity assumption for treating turbulent dissipation in convective zones is valid.

We compared this directly obtained effective viscosity with the lowest order Goodman & Oh (1997) perturbative expansion, applied to the steady state flow without forcing, and we found that this method also predicts linear scaling of the effective viscosity with period, having the same slope as predicted by the direct calculation. Again there is a significant constant offset between the perturbatively calculated turbulent viscosity and the viscosity from the direct calculation. Some part of this offset might be due to the fact that the perturbative calculation is only valid when the external perturbation period is much smaller than the convective turnover time, and the smallest value we are able to simulate is  $T \approx 0.3\tau$ .

At least part of this difference is due to actual amplitude dependence of the effective viscosity, which can be seen in figure 14 for  $\nu_{xz}^0$ . While our calculations show clear evidence of this amplitude dependence it is relatively less important than the period dependence at least in the range of amplitudes accessible to our numerical model.

To summarize, for forcing periods comparable to the local turnover time of the largest eddies ( $\tau$ ) the effective viscosity scales linearly with period and for our convective box its  $x, z$  and  $x, y$  components can be approximated by:

$$\nu_{xz}(T) \approx (0.1 + \delta_{xz}(A)) \langle v_z^2 \rangle^{1/2} H_p \min \left[ \frac{T}{2.3\tau}, 1 \right] \quad (23)$$

$$\nu_{xy}(T) \approx (0.1 + \delta_{xy}(A)) \left\langle \frac{v_x^2 + v_y^2}{2} \right\rangle^{1/2} H_p \min \left[ \frac{T}{2.3\tau}, 1 \right] \quad (24)$$

Where  $T$  is the period of the external forcing, and  $\delta_{xz}(A)$  and  $\delta_{xy}(A)$  are constant amplitude dependent offsets that are also dependent on the particular method for deriving effective viscosities.

The limited spatial resolution of our box does not allow us to reliably simulate the case of  $T \ll \tau$ . In that regime the assumptions for Kolmogorov turbulence hold and the effective viscosity should scale quadratically with the period (Goodman & Oh, 1997).

We compare the above directly calculated viscosities to a perturbative estimate of the effective viscosity (see Goodman & Oh (1997); Penev et al. (2007, 2008b)), which also predicts linear period dependence with the same slope, but with  $\delta = 0$  for all viscosity components.

The effective viscosity obtained by the perturbative calculation is approximately a factor of two larger than the corresponding effective viscosity component in Penev et al. (2008b), even though both values are found using the same method. This is expected since, if we were to define a mixing length parameter for the convective box used in this paper, its value would be  $\alpha \approx 3$ . This is approximately a factor of two larger than the mixing length parameter usually assumed for the Sun and relevant to the convective simulations used in deriving the Penev et al. (2008b) result.

The viscosity of equations 23 and 24 is closer to the Zahn (1966, 1989) prescription including the saturation period with the correction that we expect the linear loss of efficiency applies only in a limited range and for shorter periods faster loss of efficiency should apply. This might be the resolution of the apparent discrepancy between the dissipation necessary to explain tidal circularization and the red edge of the Cepheid instability strip on one hand and the observed amplitudes of the solar p-modes on the other. For small periods (of order minutes) the Kolmogorov scaling of turbulence holds and a quadratic decrease in the effective viscosity is appropriate. For long periods (of order days) the assumptions necessary for Kolmogorov cascade are not satisfied and the effective viscosity is found to scale linearly with period.

## References

- Goldreich, P. & Keeley, D. A. 1977, *ApJ*, 211, 934
- Goldreich, P. & Kumar, P. 1988, *ApJ*, 326, 462
- Goldreich, P., Murray, N., & Kumar, P. 1994, *ApJ*, 424, 466
- Goldreich, P. & Nicholson, P. D. 1977, *Icarus*, 30, 301
- Gonczi, G. 1982, *A&A*, 110, 1
- Goodman, J. & Oh, S. P. 1997, *ApJ*, 486, 403
- Malagoli, A., Cattaneo, F., & Brummell, N. H. 1990, *apjl*, 361, L33
- Meibom, S. & Mathieu, R. D. 2005, *ApJ*, 620, 970
- Penev, K., Barranco, J., & Sasselov, D. 2008a, *ArXiv e-prints*
- Penev, K., Sasselov, D., Robinson, F., & Demarque, P. 2007, *ApJ*, 655, 1166
- . 2008b, *ArXiv e-prints*
- Robinson, F. J., Demarque, P., Li, L. H., Sofia, S., Kim, Y.-C., Chan, K. L., & Guenther, D. B. 2003, *MNRAS*, 340, 923
- Sofia, S. & Chan, K. L. 1984, *apj*, 282, 550
- Stein, R. F. & Nordlund, A. 1989, *ApJ*, 342, L95
- Verbunt, F. & Phinney, E. S. 1995, *A&A*, 296, 709
- Zahn, J. P. 1966, *Ann. d’Astrophys.*, 29, 489
- Zahn, J. P. 1989, *A&A*, 220, 112